Influence of global rotation and Reynolds number on the large-scale features of a turbulent Taylor-Couette flow

Florent Ravelet, Rene Delfos, Jerry Westerweel

Influence of global rotation and Reynolds number on the large-scale features of a turbulent Taylor-Couette flow

F. Ravelet,[1,2] R. Delfos,[1] and J. Westerweel[1]

[1] *Laboratory for Aero and Hydrodynamics, Mekelweg 2, 2628 CD Delft, The Netherlands.*
[2] *IMFT, CNRS-UMR5502, Allée du Prof. C. Soula, 31400 Toulouse, France**

(Dated: Writting in progress: March 17, 2008)

We report on the torque scaling and the angular momentum transport mechanisms in a turbulent flow between two independently rotating cylinders. Depending on the angular velocity ratio, we identify two different states in the time-average or mean flow: one with a secondary flow consisting of large scale roll structures, and one without secondary flow, similar to the two flow states as found in laminar Taylor-Couette flow. Varying the angular velocity ratio of the two cylinders, while maintaining a constant shear rate, we study the transition between these two turbulent states in a quantitative manner. The transition is smooth and continuous, and resembles a supercritical bifurcation of the secondary mean flow.

Introduction. Turbulent flows are present in many applied and fundamental problems, ranging from small scales (engines, mixing) to very large scales (meteorology, convection in the earth mantle, and other astrophysical problems such as momentum transport in accretion disks). One of the several open questions is the emergence of coherent structures in turbulent flows [1]. Another interesting problem concerns the bifurcations that can arise in the turbulent regime, for instance the dynamo instability of a magnetic field in a conducting fluid [2], or multistability of the mean flow [3].

Taylor-Couette flow is the flow produced between differentially rotating coaxial cylinders [4]. When only the inner cylinder rotates, the first instability takes the form of toroidal (Taylor) vortices, and with two independently rotating cylinders, there is a host of interesting secondary bifurcations, extensively studied following the work of Coles [5] and Andereck *et al.* [6]. Moreover, it shares strong analogies with Rayleigh-Bénard convection [7, 8], which are useful to explain different torque scalings at high Reynolds numbers [9]. Finally, for some parameters relevant in astrophysical problems, the basic flow is linearly stable and can directly transit to turbulence [10].

The *turbulent* flow structure is not so well known and only few measurements are available [11]. In the case of inner cylinder rotating alone, recent direct numerical simulations suggest that vortex-like structures still exist at high Reynolds number ($Re \gtrsim 10^4$) [12, 13], whereas for counter-rotating cylinders, the turbulent flow comes from a featureless state [6]. We extend the study to high Reynolds numbers and address hereafter the question of the transition between a *turbulent* Taylor-vortex flow and this featureless turbulent flow when varying the global rotation while maintaining a constant mean shear rate.

Experimental setup. The flow is produced between two coaxial cylinders (Fig. 1). The inner one has a radius of $r_i = 110 \pm 0.05$ mm, and the outer one of $r_o = 120 \pm 0.05$ mm (gap $d = r_o - r_i = 10$ mm and gap ratio $\eta = r_i/r_o = 0.917$). Both cylinders can rotate independently, driven by two DC motors up to 10 Hz. The system is closed at both ends, with top and bottom lids rotating with the outer cylinder. The length of the inner cylinder is $L = 220$ mm (axial aspect ratio is $L/d = 22$). The torque T on the inner cylinder is measured with a rotating torque meter.

For a Newtonian fluid of kinematic viscosity ν, with the cylinders rotating at an angular speed of $\omega_{i,o}$, we use the set of parameters defined by Dubrulle *et al.* [14]: a shear Reynolds number $Re = 2/(1+\eta)\,|\eta Re_o - Re_i|$ and a "Rotation number" $Ro = (1-\eta)\,(Re_i + Re_o)/(\eta Re_o - Re_i)$, where $Re_{i,o} = (r_{i,o}\omega_{i,o}d/\nu)$ are the inner and outer Reynolds numbers respectively. With this choice, Re is based on the laminar shear rate S ($Re = Sd^2/\nu$). At 10 Hz in counter-rotation, the shear rate is around 1400 s^{-1} and $Re \simeq 1.4\times10^5$ for water. The rotation number Ro compares the mean rotation to the shear and is the inverse of a Rossby number. Its sign defines cyclonic ($Ro > 0$) or anti-cyclonic ($Ro < 0$) flow. The rotation number is zero in case of perfect counter-rotation ($r_i\omega_i = -r_o\omega_o$). Two other relevant values are $Ro_i = \eta - 1 \simeq -0.083$ and $Ro_o = (1-\eta)/\eta \simeq 0.091$ for inner and outer cylinder rotating alone, respectively. Finally, let us recall that at high η, *i.e.* $(1-\eta) \ll 1$, the flow is linearly unstable for $-1 < Ro < Ro_o$ [14, 15].

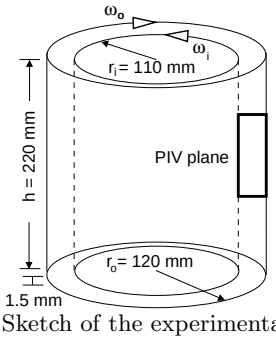

FIG. 1: Sketch of the experimental setup.

We measure the three components of the velocity by stereoscopic PIV [16] in a vertical plane normal to the mean flow (Fig. 1). The light-sheet thickness is 0.5 mm,

which is observed from both sides using two double-frame CCD-cameras on Scheimpflug mounts. The tracer particles are 20 μm fluorescent (rhodamine) spheres. The field of view is 11×25 mm^2. For the calibration procedure we use a thin transparent grid, attached to a rotating and translating micro-traverse. The PIV images are processed with DaVis 7.2.

Scaling of the torque. We present in Fig. 2 the friction factor $C_f = T/(2\pi\rho r_i^2 LU^2) \propto G/Re^2$, with $U = Sd$ and $G = T/(\rho L\nu^2)$, as a function of Re for three particular rotation (Ro) numbers, corresponding to inner cylinder rotating alone, exact counter-rotation and outer cylinder rotating alone. At low Re, the three curves collapse on a Re^{-1} curve. This characterizes the laminar regime where the torque is proportional to the shear rate on which the Reynolds number is based.

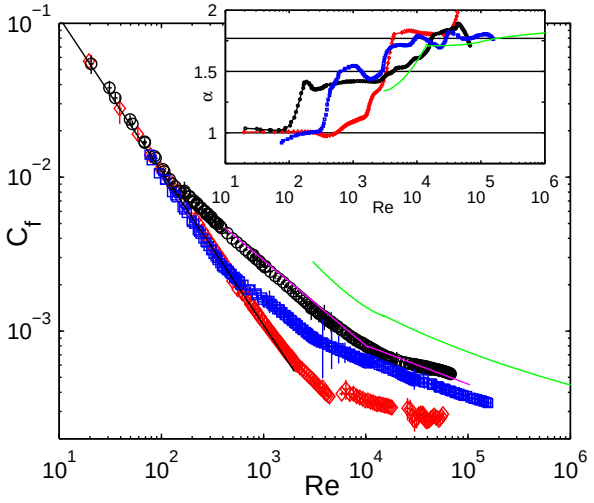

FIG. 2: Friction factor C_f vs. Re for $Ro_i = \eta - 1$ (black ○), $Ro_c = 0$ (blue □) and $Ro_o = (1-\eta)/\eta$ (red ⋄). Relative error on Re: ±5%, absolute error on torque: ±0.02 Nm. Inset: local exponent α such that $C_f \propto Re^{\alpha-2}$, computed as $2 + d\log(C_f)/d\log(Re)$, for $Ro_i = \eta - 1$ (black), $Ro_c = 0$ (blue)and $Ro_o = (1-\eta)/\eta$ (red). Solid green line: fit of Lewis data, eq. 3 of Ref. [9], for Ro_i and $\eta = 0.724$. Solid magenta line: eq. 10 of Ref. [17]. Solid black line: laminar friction factor $C_f = 1/(\eta Re)$.

For $Ro_i = \eta - 1$, one can notice a transition to a different regime at $Re_{ci} \simeq 140$ (theoretical threshold $Re = 150$ [15]). This corresponds to the linear instability of the basic flow, leading in this case to the growth of laminar Taylor vortices. The friction factor is then supposed to scale as $Re^{-1/2}$ ($\alpha = 3/2$), which is the case here (see inset in Fig. 2). For exact counter-rotation ($Ro_c = 0$), the first instability threshold is $Re_{cc} \simeq 400$. This is somewhat lower than the theoretical prediction $Re = 515$ [15], which is probably due to our finite aspect-ratio. The Taylor-Couette flow with outer cylinder rotating alone ($Ro_o = (1-\eta)/\eta$) is linearly stable whatever Re. The experimental flow is still laminar at $Re \simeq 4000$.

Further increase of the shear Reynolds number also increases the local exponent (see inset in Fig. 2). For $Ro_i = \eta - 1$, it gradually rises from $\alpha \simeq 1.5$ at $Re \simeq 200$ to $\alpha \simeq 1.8$ at $Re \simeq 10^5$. The order of magnitude of these values agree with the results of Lewis *et al* [9], though a direct comparison is difficult, owing to the different gap ratios of the experiments. The local exponent is supposed to approach a value of 2 for increasing gap ratio. Dubrulle & Hersant [7] attribute the increase of α to logarithmic corrections, whereas Eckhardt *et al* [8] attribute the increase of α to a balance between a boundary-layer/hairpin contribution in $Re^{3/2}$ and a bulk contribution in Re^2. The case of perfect counter-rotation shows a plateau at $\alpha \simeq 1.5$ and a sharp increase of the local exponent to $\alpha \simeq 1.75$ at $Re_{tc} \simeq 3200$, possibly tracing back a secondary transition. The local exponent then seems to increase gradually. Finally, for $Ro_o = (1-\eta)/\eta$, the flow directly transits from a laminar state to a turbulent state with a local exponent around $\alpha = 1.77$ at $4000 \lesssim Re_{to} \simeq 5000$. One can finally notice that at the same shear Reynolds number, for $Re \geq 10^4$ the local exponents for the three rotation numbers are equal within ±0.1 and that the torque with inner cylinder rotating alone is greater than the torque in counter-rotation, this latter being greater than the torque for outer cylinder alone. Please note that the dimensional values of the torque when only the outer cylinder rotates are very small and difficult to measure accurately, and that these become of the same order as the end effect corrections that we have to take into account.

We now address the question of the transition between these different turbulent states at a constant shear Reynolds number.

Mean flow bifurcation. The presence of vortex-like structures at high Reynolds number ($Re \gtrsim 10^4$) in turbulent Taylor-Couette flow with the inner cylinder rotating alone is confirmed in our experiment through stereoscopic PIV measurements [18]. The time-averaged flow shows strong secondary mean flow in the form of vortices. The time-averaged angular velocity profile is almost flat and the angular momentum transport is then mainly determined by these coherent structures; their contribution corresponds to 75% of the total transport, with the remaining 25% being done by correlated fluctuations. On the contrary, in the case of perfect counter-rotation there is no mean secondary flow, and the angular momentum is completely transported by strong fluctuating structures more similar to those in plane turbulent Couette flows. In that case, the correlation coefficient between radial and azimuthal fluctuations is 0.4 [18].

To characterize the transition between these two regimes, we first consider the global torque measurements. We plot in Fig. 3 the friction factor normalised by the torque for inner cylinder rotating alone as a function of the rotation number (Ro), for a constant shear Reynolds number in the turbulent regime ($Re = 1.4 \times 10^4$). We first identify the hierarchy of flow states:

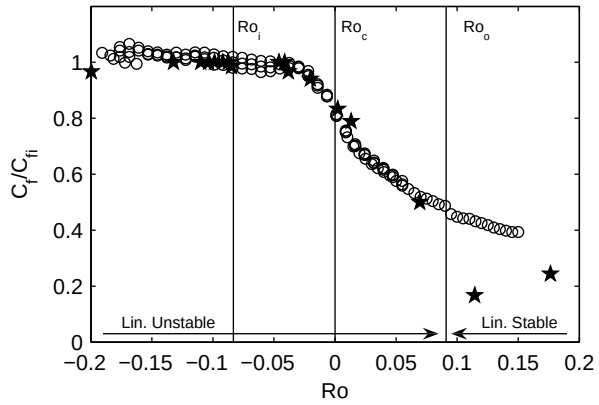

FIG. 3: C_f, normalized by $C_{fi} = C_f(Ro_i)$, vs. Ro at a constant shear Reynolds number $Re = 1.4 \times 10^4$. ($\star$: data from Wendt [19] at various $\eta \geq 0.85$).

the torque in counter-rotation (Ro_c) is approximately 80% of $C_f(Ro_i)$, and the torque with outer cylinder rotating alone (Ro_o) is approximately 50% of $C_f(Ro_i)$. These values compare well with the few available data, compiled by Dubrulle *et al* [14]. The curve shows a plateau of constant torque from $Ro = -0.2$, *i.*e. when both cylinders rotate in the same direction with the inner cylinder rotating faster than the outer cylinder, to $Ro \simeq -0.035$, *i.*e. with a small amount of counter-rotation with the inner cylinder still rotating faster than the outer cylinder. The torque then monotonically decreases when accelerating the outer cylinder, with an inflexion point at Ro_c. The transition is continuous and smooth, and the effect of rotating the outer cylinder starts to be seen on the torque very close to perfect counter-rotation.

We now focus on the changes observed in the mean flow. To extract quantitative data from the PIV measurements, we use the following model for the stream function of the secondary flow: $\Psi = \sin[\pi(r-r_i)/d] \times \{A_1 \sin[\pi(z-z_0)/\ell] + A_3 \sin[3\pi(z-z_0)/\ell]\}$, with free parameters A_1, A_3, ℓ and z_0. This corresponds to alternating rolls, with a wavelength of 2ℓ and a maximum radial velocity given by $\pi(A_1/\ell + 3A_3/\ell)$. It is implicitly assumed that the flow is developed sufficiently to restore the axisymmetry, which is *a posteriori* checked. We previously tried a single mode in axial direction, but it appears that using also the third harmonic improves the matching between the model and the actual velocity fields, especially close to Ro_i (see Fig. 4).

We first discuss the case $\{Ro = Ro_i; Re = 1.4{\times}10^4\}$. A sequence of 4,000 PIV images at a data rate of 3.7 Hz is taken, and 20 consecutive PIV images, *i.e.* approximately 11 cylinder revolutions, are sufficient to obtain a reliable estimate of the mean flow [13]. It is known that for the first transition the observed flow state can depend on the initial conditions [5]. When starting the inner cylinder from rest and accelerating it to 2 Hz in 20 s, the vortices grow very fast, reach a value with a velocity amplitude of 0.08 ms^{-1}, and then decay to become stabilized at a value around 0.074 ms^{-1} after 400 seconds. Transients are thus also very long in turbulent Taylor-vortex flows. For slower accelerations, the first vortices are weaker and have a larger length scale, before reaching the same final state. The final length scale of the vortices for Ro_i is about 1.2 times the gap width, consistent with data from Bilson *et al.* [12].

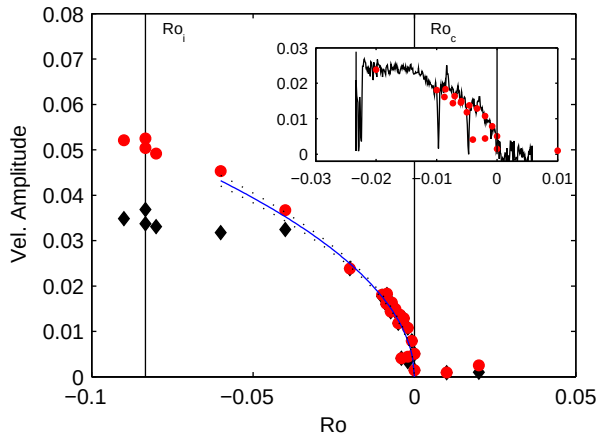

FIG. 4: Secondary flow amplitude *vs.* rotation number (Ro) at constant shear rate. Black ($\diamond$): model with fundamental mode only, and red ($\circ$): complete model with third harmonic. Solid line is a fit of the form $A = a(-Ro)^{1/2}$. Inset: zoom close to counter-rotation, combined with results from a continuous experiment (see text).

In a subsequent measurement we start from $\{Ro = Ro_i; Re = 1.4{\times}10^4\}$ and vary the rotation number in small increments, while maintaining a constant shear rate. We allow the system to spend 20 minutes in each state before acquiring PIV data. We verify that the fit parameters are stationary, and compute them using the average of the full PIV data set at each Ro. The results are plotted in Fig. 4. Please note that Ro has been varied both with increasing and decreasing values, to check for a possible hysteresis. All points fall on a single curve; the transition is smooth and without hysteresis. For $Ro \geq 0$, the fitted modes have zero or negligible amplitudes, since there are no flow structures in the time-average field [18]. One can notice that as soon as $Ro < 0$, *i.e.* as soon as the inner cylinder starts to rotate faster than the outer cylinder, vortices begin to grow. We plot in Fig. 4 the velocity amplitudes associated with the simple model (single mode $\diamond$), and with the complete model (modes 1 and 3, $\circ$). Very close to $Ro = 0$, the two models coincide: $A_3 \simeq 0$ and the secondary mean flow is well described by pure sinusoidal structures. For $Ro \lesssim -0.04$, the vortices start to have elongated shapes, with large cores and small regions of large radial motions in between adjacent vortices; the third mode is then necessary to adequately describe the secondary flow. The first mode becomes saturated in this region. Finally, we give in Fig. 4 a fit of the amplitudes close to $Ro = 0$ of the form: $A = a\,(-Ro)^{1/2}$. The velocity amplitude of the vortex behaves like the

square root of the distance to $Ro = 0$, a situation reminiscent to a classical supercritical bifurcation, with A as order parameter, and Ro as control parameter.

We also performed a *continuous* experiment, i.e. varying the rotation number quasi-statically from Ro=0.004 to Ro=–0.0250 in 3000 s. The amplitude of the mean secondary flow, computed on sequences of 20 images, is plotted in the inset of Fig. 4. The curve follows the static experiments (given by the single points), but some downward peaks can be noticed. We checked that these are not the result of a fitting error, and indeed correspond to the occasional disappearance of the vortices. They could correspond to the Eckhaus instability of the pattern wavelength. Still, the measurements are done at a fixed position in space. Though the very long time-averaged series lead to well-established stationary axisymmetric states, it is possible that the instantaneous whole flow consists of different regions. Further investigation including time-resolved single-point measurements or flow visualizations need to be done to verify this possibility.

Conclusion The rotation has some obvious effects on the torque scaling. Whereas the local exponent evolves in a smooth way for inner cylinder rotating alone, the counter-rotating case exhibits two sharp transitions, from $\alpha = 1$ to $\alpha \simeq 1.5$ and then to $\alpha \simeq 1.75$. We also notice that the second transition for counter-rotation Re_{tc} is close to the threshold Re_{to} of turbulence onset for outer cylinder rotating alone. A way to analyze the flow is to decompose it into two regions, dominated by each cylinder and separated by a neutral surface [15]. For Ro_c, we could thus infer that at low Re, the inner zone dominates, and at higher Re, the outer zone dominates.

The rotation number (Ro) is thus a secondary control parameter. It is very tempting to use the classical formalism of bifurcations and instabilities to study the transition between featureless turbulence and turbulent Taylor-vortex flow at constant Re, which seems to be supercritical; the threshold for the onset of coherent structures in the mean flow is Ro_c. For anticyclonic flows ($Ro < 0$), the transport is dominated by large scale coherent structures, whereas for cyclonic flows ($Ro > 0$), it is dominated by correlated fluctuations reminiscent to thermal plumes, with no viscous contribution at all for $Ro \leq 0$ but a few 10% at Ro_o [18]. Counter-rotation Ro_c corresponds to an inflexion point in the torque curve. The perfect counter-rotating case thus seems to be a peculiar boundary for the turbulent Taylor-Couette flow. One last remark is that rotation number $Ro = 0$ is also the threshold for linear instability for rotating plane Couette flow, which exactly corresponds to the limit of a Taylor-Couette flow with vanishing curvature [20].

We are particularly indebted to J.R. Bodde, C. Gerritsen and W. Tax for building up and piloting the experiment. We have benefited of very fruitful discussions with A. Chiffaudel, F. Daviaud, B. Dubrulle and B. Eckhardt.

* Electronic address: florent.ravelet@ensta.org

[1] P. J. Holmes, J. L. Lumley, and G. Berkooz. *Turbulence, Coherent Structures, Dynamical Systems and Symmetry.* Cambridge University Press, 1996.

[2] R. Monchaux et al. Generation of magnetic field by dynamo action in a turbulent flow of liquid sodium. *Phys. Rev. Lett.*, 98:044502, 2007.

[3] N. Mujica and D. P. Lathrop. Hysteretic gravity-wave bifurcation in a highly turbulent swirling flow. *J. Fluid Mech.*, 551:49, 2006.

[4] M. Couette. Etude sur le frottement des liquids. *Ann. Chim. Phys.*, 21:433, 1890.

[5] D. Coles. Transition in circular Couette flow. *J. Fluid Mech.*, 21:385, 1965.

[6] C. D. Andereck, S. S. Liu, and H. L. Swinney. Flow regimes in a circular Couette system with independently rotating cylinders. *J. Fluid Mech.*, 164:155, 1986.

[7] B. Dubrulle and F. Hersant. Momentum transport and torque scaling in Taylor-Couette flow from an analogy with turbulent convection. *Euro. Phys. J. B*, 26:379, 2002.

[8] B. Eckhardt, S. Grossmann, and D. Lohse. Torque scaling in Taylor-Couette flow between independently rotating cylinders. *J. Fluid Mech.*, 581:221, 2007.

[9] G. S. Lewis and Harry L. Swinney. Velocity structure functions, scaling, and transitions in high-Reynolds-number Couette-Taylor flow. *Phys. Rev. E*, 59:5457, 1999.

[10] F. Hersant, B. Dubrulle, and J.-M. Huré. Turbulence in circumstellar disks. *A&A*, 429:531, 2005.

[11] S. T. Wereley and R. M. Lueptow. Spatio-temporal character of non-wavy and wavy Taylor-Couette flow. *J. Fluid Mech.*, 364:59, 1998.

[12] M. Bilson and K. Bremhorst. Direct numerical simulation of turbulent Taylor-Couette flow. *J. Fluid Mech.*, 579:227, 2007.

[13] S. Dong. Direct numerical simulation of turbulent Taylor-Couette flow. *J. Fluid Mech.*, 587:373, 2007.

[14] B. Dubrulle et al. Stability and turbulent transport in Taylor-Couette flow from analysis of experimental data. *Phys. Fluids*, 17:095103, 2005.

[15] A. Esser and S. Grossmann. Analytic expression for Taylor-Couette stability boundary. *Phys. Fluids*, 8:1814, 1996.

[16] A. K. Prasad. Stereoscopic particle image velocimetry. *Exp. Fluids*, 29:103, 2000.

[17] A. Racina and M. Kind. Specific power input and local micromixing times in turbulent Taylor-Couette flow. *Exp. Fluids*, 41:513, 2006.

[18] F. Ravelet, R. Delfos, and J. Westerweel. Experimental studies of turbulent Taylor-Couette flows. In *Proc. 5th Int. Symp. on Turbulence and Shear Flow Phenomena, Munich*, page 1211, 2007. http://arxiv.org/abs/0707.1414.

[19] F. Wendt. Turbulente Strömungen zwischen zwei rotierenden konaxialen Zylindern. *Arch. Appl. Mech.*, 4:577–595, 1933.

[20] K. Hiwatashi, P. H. Alfredsson, N. Tillmark, and M. Nagata. Experimental observations of instabilities in rotating plane Couette flow. *Phys. Fluids*, 19:048103, 2007.